Heliyon 10 (2024) e25452

Contents lists available at ScienceDirect

Heliyon

journal homepage: www.cell.com/heliyon

Research article

Effect of laser remelting power on the microstructure and properties of vanadizing layer on AISI 52100 steel pin shaft

Zhizhong Zeng, Jian Shang *, Dan Lin

School of Materials Science and Engineering, Liaoning University of Technology, Jinzhou, China

ARTICLE INFO

Keywords:
Laser remelting
Pack cementation
Vanadizing
Microstructure and properties

ABSTRACT

The surface of AISI 52100 steel was pre-treated by laser remelting with different powers, and the vanadizing layer were prepared on remelted steel by pack cementation. The microstructure and properties of vanadizing layer were investigated by XRD, microhardness tester, metallographic microscope, scanning electron microscope, energy dispersive spectrometer, friction and wear tester. The critical load L_c was determined by observing the micro-scratch morphology of scratches through micro-scratch experiments, and its wear performance was studied. The results show that the hardness of remelting zone increase with the increase of laser power. When the laser power is 500 W, the microhardness is 424.6 $HV_{0.2}$. The vanadizing layer formed on the remelting surfaces is uniform and dense. The layers are mainly composed of VC_x phase and α-Fe/α′-Fe phase, the VC phase has the preferred orientation of (200) and (111) planes. There is a good metallurgical bonding between the vanadizing layer and the steel , and the thickness is 2.7 μm–12.15 μm, the microhardness is 2050.7 $HV_{0.2}$–2350.9 $HV_{0.2}$. When the laser remelting power is 300 W, the vanadizing layer is better in thickness, microhardness and average friction coefficient, the bonding force Lc between the vanadizing layer and the substrate is about 41.59 N, and the main failure mode is the spalling of the vanadizing layer. It can be concluded that laser remelting pre-treatment can greatly improve the hardness and wear resistance.

1. Introduction

1.1. Preface

AISI 52100 steel has high hardness, high strength, good wear resistance and high contact fatigue strength after quenching and tempering. Because of its good performance, it is often used to manufacture molds and precision measuring tools [1–4]. AISI 52100 steel is one of the most widely used materials in the field of bearin, however, after traditional heat treatment, the transformation of retained austenite to untempered martensite will occur in the process of long-term service of AISI 52100 steel, resulting in problems such as reduced hardness, loss of precision and decreased fatigue life [5–7]. Strengthening process is used to improve the surface properties of steel, increase the hardness and wear resistance of steel and prolong its service life, the strengthening methods mainly include laser surface treatment, ion implantation, thermal spraying, vapor deposition, chemical heat treatment, multi-element co-penetration, etc. [8–11]. Y Yang et al. [12]prepared the WC/Ni-based coating on AISI H13 steel by laser cladding. The effects of different laser energy densities on the coating were studied. The results showed that the wear resistance and microhardness did not

* Corresponding author.
E-mail address: shangbahao@163.com (J. Shang).

https://doi.org/10.1016/j.heliyon.2024.e25452
Received 31 October 2023; Received in revised form 21 January 2024; Accepted 26 January 2024
Available online 2 February 2024
2405-8440/© 2024 The Authors. Published by Elsevier Ltd. This is an open access article under the CC BY-NC-ND license (http://creativecommons.org/licenses/by-nc-nd/4.0/).

change significantly with the increase of laser energy density, and the microstructure uniformity of the coating was better. When the energy density was 1500 J/mm, the microstructure uniformity of the coating was best. N Zhao et al. [13] used AISI 52100 and high-purity tantalum plates as raw materials to prepare a high-hardness and corrosion-resistant TaC–Fe reinforced layer on the surface of AISI 52100 steel by in-situ hot pressing at a temperature of 1000 °C and a pressure of 40 MPa. It is found that the phase composition is mainly TaC and a small amount of α-Fe phase. The obtained TaC–Fe reinforced layer has good metallurgical bonding with AISI 52100, and the bonding force is more than 100 N. In the electrolyte solution, the corrosion rate of the TaC–Fe reinforced layer is only 19 % of that of AISI 52100, and the protection efficiency is 81 %. The TaC–Fe reinforced layer has good protection and anti-corrosion effect on AISI 52100. J Chen et al. [14] conducted laser treatment on the surface of AISI 52100, simulated the temperature field to explore the influence of different depths on the peak temperature, and studied the microstructure changes of the laser hardened layer. The results show that the peak temperature trend increases exponentially with the decrease of depth. At the high peak temperature, the grains are relatively coarse, and at the deeper position of the hardened layer, the austenite grain size is slightly reduced. T Dong et al. [15] prepared AlCoCrFeNi HEA coating on AISI 1045 steel by plasma spraying technology, and then the coating was remelted by laser. The oxidation experiment was carried out and the effects of laser remelting on the coating were compared. The results show that the laser remelting does not change the phase composition of the coating, and porosity of the coating decreases from 4.8 % to 0.3 %. J Shang et al. [16] in order to improve the surface properties of AISI H13 steel, the vanadizing layer, tantalizing layer and niobizing layer were prepared by pack cementation method at 940 °C for 7 h, and then the high temperature friction and wear test were carried out to characterize properties of different layers. The results show that the vanadizing layer and the niobizing layer can improve the wear resistance and the hot melt loss resistance. The vanadizing is an effective method to improve the service life of the H13 steel. L. Meng et al. [17] studied the vanadizing layer on the surface of AISI 52100 steel with adding rare earth by pack cementation. The results show that the vanadizing layer is mainly composed of VC_X and α-Fe. The thickness and hardness of the vanadizing layer increase with the increase of holding time. The thickness and hardness of the vanadizing layer are 4.65–12.65 μm and 1892.3–2698.6 HV, respectively.

In this paper, two kinds of treating methods are mainly used. First, the AISI 52100 steel is subjected to laser remelting pre-treatment, and then the vanadizing treatment is used to further improve the properties. Laser remelting pretreatment can be considered as a quick heat treatment and grain refine method under the proper parameters, so and more fine martensite is obtained. The grain-refined structure can be favor to the diffusion. The main process is to compare the microstructure and properties of vanadizing layer with or without of the laser remelting pretreatment and explore a new treating method for repair application.

2. Experimental materials and methods

The material used in this experiment is AISI 52100 steel after spheroidizing annealing treatment. The specific chemical composition (wt. %) was detected by direct reading spectrometer (Q4 Bruker) as shown in Table 1. The AISI 52100 steel bar is cut into a round block with a size of Φ15mm × 4 mm, and the Φ15mm surface disk is used as the sample surface. The (Shanxi, China) YLK-3000 fiber laser is used, the scanning speed is 2 mm/s, the overlap rate is 1 mm, the laser radius is 1.2mm–1.5 mm, and the laser remelting treatment with power of 0 W, 100 W, 200 W, 300 W, 400 W, 500 W is carried out on the surface of AISI 52100 steel. The 120# −600# sandpapers are used to grind surface to bright and scratch-free, and then are ultrasonically treated in anhydrous ethanol solution and dried. Subsequently, the powder pack cementation method was used for vanadizing treatment. The composition of the mixing agent was 5 % NH_4Cl, 47.5 % Al_2O_3, and 47.5 % V–Fe. The mixed agent was put into the tank and was placed in a box-type furnace. The heating temperature was 940 °C and the holding time was 5 h [17].

The phases of laser remelting and vanadizing samples were analyzed by D/max-2500/pc X-ray diffractometer (XRD). The Cu target was used, the scanning angle was 30°–90° and scanning speed was 8°/min at 100 mA and 40 kV. The microstructure was analyzed by Axio Vert.21 Al metallographic microscope. The hardness of the layer was measured by HVS-1000 automatic microhardness tester. The selected load was 0.2 N, the holding time was 10 s, and each sample was tested with 7 points. The microstructure and element distribution of prepared layers were analyzed by Zeiss Sigma 500 scanning electron microscope (SEM) and Oxford AZtecX-Max 50 energy spectrometer. The friction and wear experiments were carried out by using the HT-1000 friction and wear tester. The Si_3N_4 ceramic ball (Φ6.35 mm) was selected as the couple. The sliding conditions are room temperature, 15 min, 10 N and 500 r/min speed. The micro-scratch test was carried out by using the MFT-4000 material surface performance tester. The critical load is estimated to be 0–100 N, the scratch length is 3 mm, and the loading rate is 100 N/min.

3. Experimental results and analysis

3.1. Sectional structure of laser remelting zone with different power

From Fig. 1 (a), (b), we can see that the laser remelting zone was not obvious The matrix structure was ferrite and pearlite mainly. With the increase of laser remelting power, the area of remelting zone gradually increased, see Fig. 1 (c)-(f). The structure in the

Table 1
Tempered chemical composition of AISI 52100 bearing (wt.%).

Element	C	Mn	Si	S	Cr	P	Ni	Fe
Content	0.96	0.27	0.18	0.01	1.43	0.017	0.21	Bal

remelting zone is more fine and the matrix structure is composed of ferrite and pearlite. Compared with the microstructures, there are three obvious differences in the sectional metallographic microstructure photos, the remelting zone, the matrix structure and the black inlay. The black inlay is mainly epoxy resin, which only plays the role of fixing the sample, the resin shows a black image under the metallographic microscope. According to metallographic observation, the laser heating region can be divided into three sub-regions from inside to outside according to different depths, namely, the fully hardened region, the transition region and the heat affected region. The surface area (fully hardened area) of the laser remelted zone is composed of martensite, austenite and residual granular carbide.

After laser remelting, the sample is cooled rapidly by the heat conduction of the matrix, and the austenite is transformed into martensite. With an increase of temperature, the microstructure becomes completely austenitic, which subsequently after cooling partially convert to martensite and austenite [18]. In the middle is the transitional region, which consists of martensite, residual austenite, carbide and ferrite. This region should be only partially austenitized, and therefore some ferrite remains. The far right of the sample is the heat affected zone, and the microstructure has no obvious change, similar to that of the matrix [19]. It can be seen that under different power laser remelting treatment, a remelting zone with fine grain size can be obtained [20].

3.2. Microhardness analysis of different power laser remelting zone

Fig. 2 is the microhardness of surface layer treated by laser remelting under different laser powers. In order to reduce the error, each group of data uses 7 microscopic data points, and the average value is taken as the data value of the group. In the laser remelting process, the heat dissipation of the sample is faster than that of the laser remelting zone, and the solidification speed is also faster than that of the laser remelting zone. The crystal grains gradually decrease from the sample to the heat-affected zone to the remelting zone. With the increase of laser power, the area of the remelting zone on the surface of the sample gradually increases, and more fine martensite is obtained to gradually increase the hardness [21,22]. It can be seen from the figure that with the increase of laser remelting power, the microhardness gradually increases. Among them, the hardness after laser remelting treatment with a power of

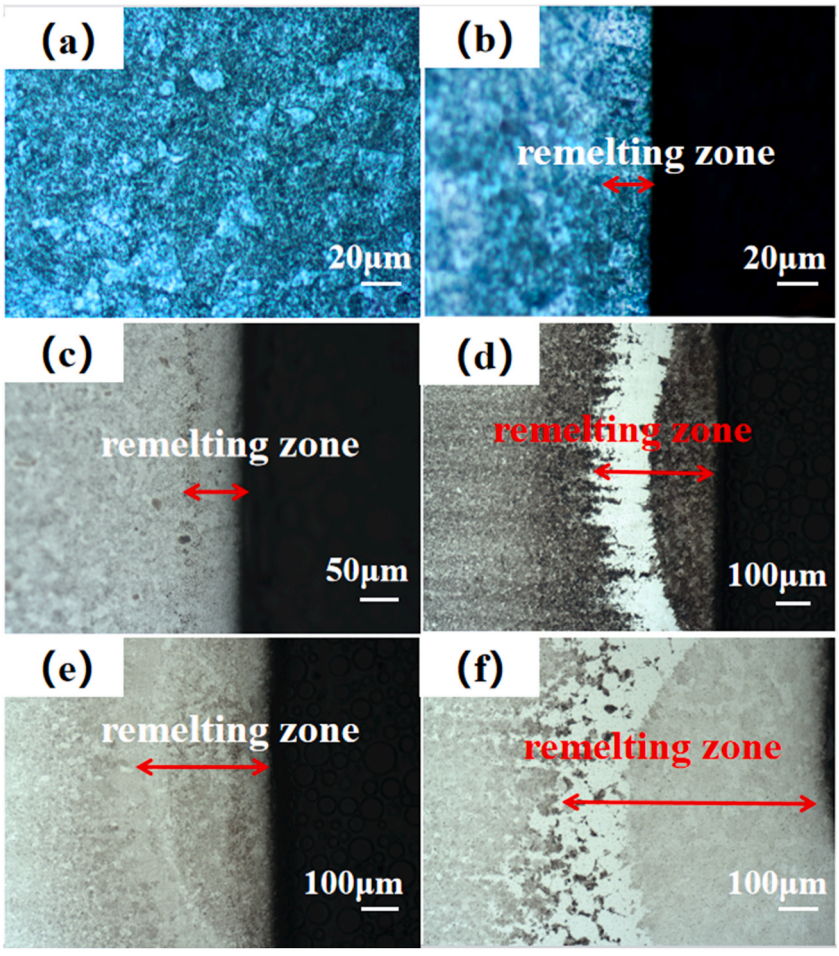

Fig. 1. Morphology of laser remelting zone with different powers. (**a**) 0 W(**b**) 100 W (**c**) 200 W (**d**) 300 W (**e**) 400 W (**f**) 500 W.

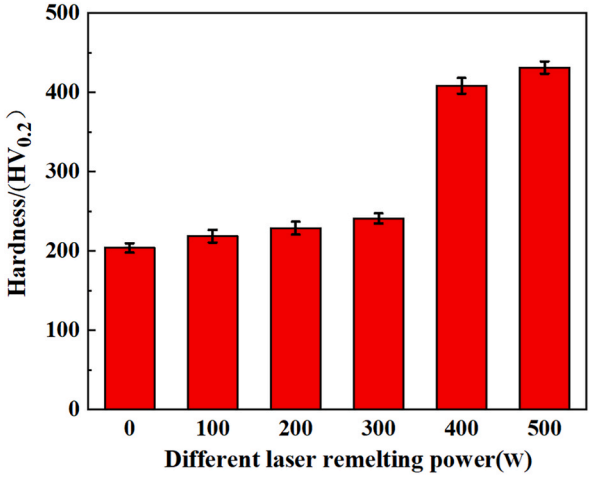

Fig. 2. Microhardness of laser remelting zone with different powers.

300 W to the hardness value after laser remelting treatment with a power of 400 W has the largest growth, and then the maximum is 424.6 $HV_{0.2}$ when the power is 500 W laser remelting treatment.

3.3. XRD phase analysis of surface of laser remelting zone with different power

Fig. 3 (a) shows the XRD analysis of laser remelting zone with different powers. It can be seen that the phase of AISI 52100 steel after laser remelting is mainly α'-Fe, which is not changed compared with matrix phase. Therefore, it is concluded that laser remelting does not change the phase composition of matrix. Fig. 3 (b) shows that the α'-Fe peak shifts to the right with the increase of power between 40° and 50°. And it is proved that the grains are more fine with increase of laser remelting power.

3.4. The cross section structure and thickness of vanadizing layer after laser remelting with different powers

As can be seen in Fig. 4 (a) - (f), when the laser remelting with different powers, the white layer can be formed in the remelting surface with different thickness. And there is a clear interface between the vanadizing layer and the matrix. When laser remelting with power of 500 W, the layer is nonuniform. The morphology of vanadizing layer after laser remelting treatment with 0 W, 300 W, and 400 W is better. The layer surface is smooth and the thickness is uniform, and the layer pre-treated by 300 W laser remelting is the thickest.

Fig. 5 shows the thickness of the vanadizing layer under different laser remelting power, the same heating temperature and holding time. The thickness of the vanadizing layer is measured by metallographic photographs. It can be seen from the thickness histogram that the thickness of the vanadizing layer decreases with the increase of laser remelting power, but the thickness of the vanadizing layer increases at 300 W, and then decreases again. The thickness range of the vanadizing layer is 2.7 μm–12.15 μm. Among them, the maximum thickness of the vanadizing layer reaches 12.15 μm, which is the vanadizing workpiece treated by laser remelting with a

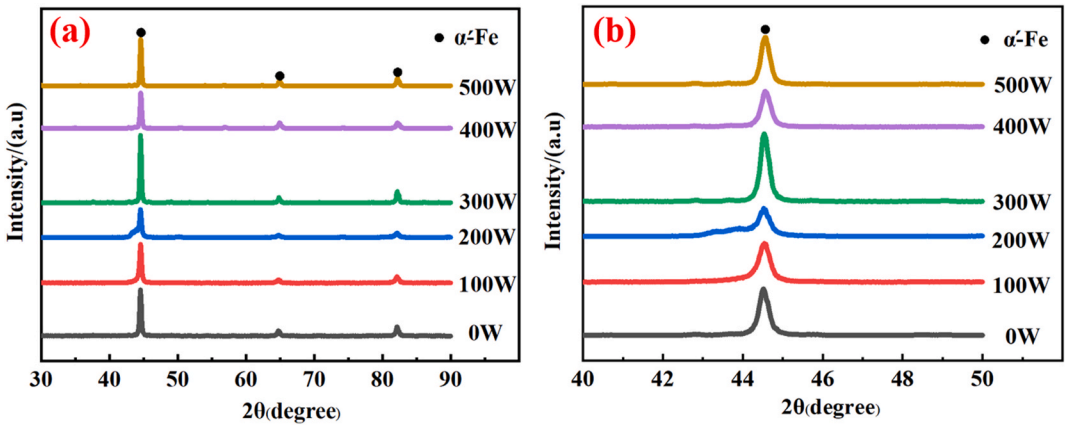

Fig. 3. XRD patterns of laser remelting zone with different powers (a) 30°–90° (b) 40°–50°.

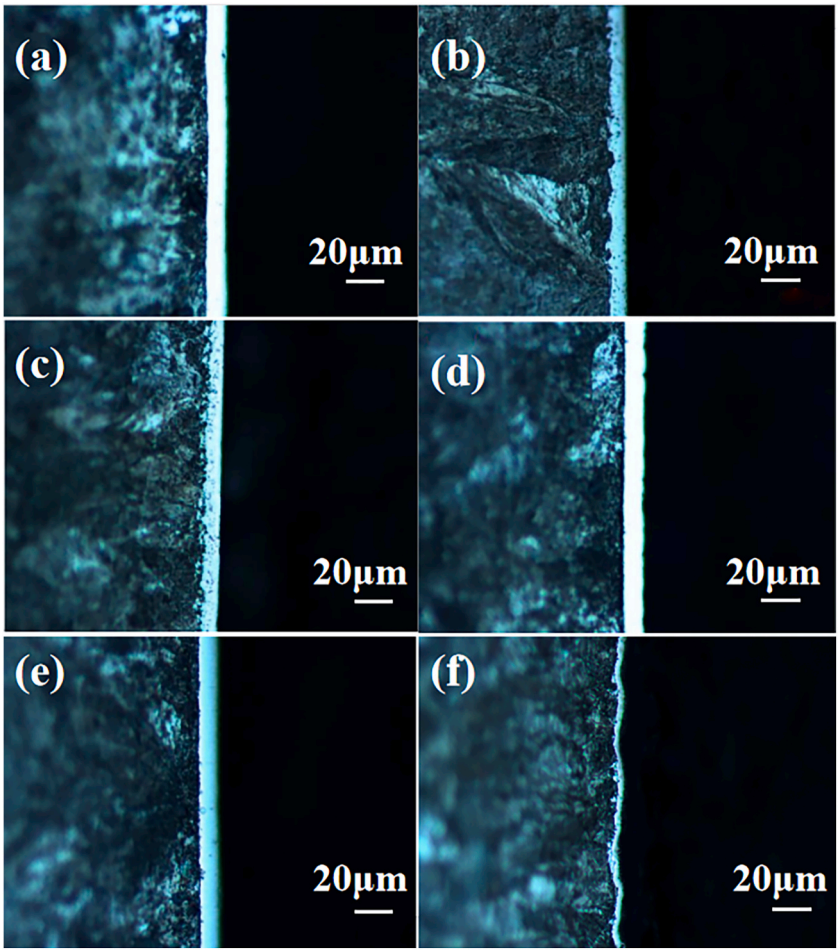

Fig. 4. Morphology of vanadizing layer after laser remelting with different powers. (**a**) 0 W (**b**) 100 W (**c**) 200 W (**d**) 300 W (**e**) 400 W (**f**) 500 W

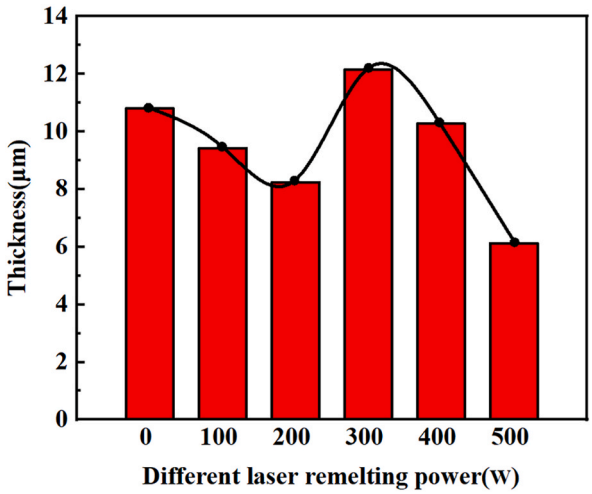

Fig. 5. Thickness of vanadizing layer after laser remelting with different powers.

power of 300 W. After laser remelting with a power of 500 W, the thickness of the vanadizing layer is the thinnest, reaching 2.7 μm, which is the same as the results shown in the metallographic photograph.

3.5. Microhardness of vanadizing layer after different power laser remelting

Fig. 6 is the hardness value of vanadizing layer under different laser remelting power, the same heating temperature and holding time. Each group of data adopts multiple microscopic data points, removes a maximum value and a minimum value, and then calculates the average value as the data value of the group, so as to reduce the error. After vanadizing treatment, a hard layer containing VC_x is formed on the surface, and the microhardness of the sample surface increases notably. From the diagram, it can be seen that with the increase of laser remelting power, the microhardness of the vanadizing layer increases first and then decreases, and the range of hardness value fluctuation is 2050.7 $HV_{0.2}$–2350.9 $HV_{0.2}$. When the laser remelting power is 300 W, the microhardness of the vanadizing layer reaches the maximum value of 2350.9$HV_{0.2}$. At this time, the mechanical properties of the vanadizing layer are the best. When the power is 0 W, the hardness value of the vanadizing layer is 2050.7 $HV_{0.2}$.

3.6. XRD phase analysis of vanadizing layer after different power laser remelting

The phase of the infiltrated layer in Fig. 7 (a) is mainly composed of α-Fe and VC_x, judging from the intensity of the diffraction peaks, the VC phase has the preferred orientation of the (200) and (111) surfaces. Among them, x (x = 0.83–0.88) represents the C/V atomic ratio, and VC_x represents a variety of vanadizing carbides, which may be VC, V_2C, V_8C_7, etc. [23] From Fig. 7 (b), it can be seen that there are some adjacent small peaks in the permeable layer near the (220) crystal plane, indicating that there is more than one phase, corresponding to Ref. [23]. VC, V_8C_7, V_6C_5 diffraction peaks are very close and difficult to distinguish. Oliveira et al. [24] refer to V carbides as VC or V_8C_7. During the time of discontinuous layer growth to continuous compact layer, Fe and C in the matrix pass through the discontinuous layer to the outer surface of the layer by the chemical potential gradient, in which C or Fe forms compounds with the active atoms on the surface of the layer to make the layer grow until the layer grows to a continuous compact state. Therefore, it is inferred that the infiltrated layer formed on the surface may be mainly composed of ordered VC phase and disordered VC_x phase, which contains a small amount of α-Fe phase. Because the carbon atoms forming the vanadizing carbide coating are derived from the sample and combine with the active vanadizing atoms to form vanadizing carbide compounds. Because the carbon atoms are in a dynamic equilibrium state, that is, from the interface between the coating and the sample to the surface, the C/V atomic ratio is different.

3.7. Scanning electron microscopy and energy spectrum analysis of vanadizing layer after different power laser remelting.

Fig. 8 (a) shows the morphology of the vanadizing layer after laser remelting at a power of 0 W. The main elements of the vanadizing layer are Fe and V, and there is obvious planar contact between the vanadizing layer and the sample. The distribution of vanadizing in the layer is relatively uniform. Since the diffusion agent does not contain carbon, it can be concluded that the carbon in the diffusion layer comes from the carbon in the matrix. This indicates that the outward diffusion of carbon atoms has been combined with the active vanadizing atoms to form a new vanadizing layer. At the junction of the matrix and the layer, the iron content increases with the increase of the depth of the layer, while the vanadizing content decreases rapidly with the increase of the depth of the layer. Therefore, there is a phenomenon of mutual penetration at the interface between the matrix and the diffusion layer, which leads to the metallurgical bonding between the matrix and the diffusion layer.

Fig. 8 (b)–(f) are the SEM images of the vanadizing layer of AISI 52100 steel after laser remelting with power of 100 W, 200 W, 300 W, 400 W and 500 W, respectively. After comparative analysis, it can be clearly seen that the thickness of the vanadizing layer after laser remelting with power of 300 W is dense and uniform, while the morphology of the vanadizing layer after laser remelting with

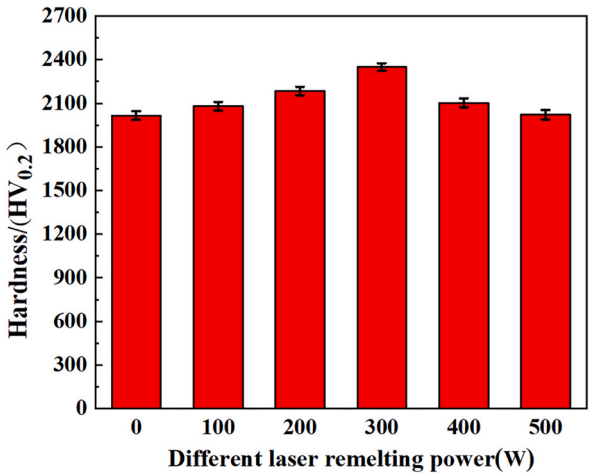

Fig. 6. Hardness of vanadizing layer after laser remelting with different powers.

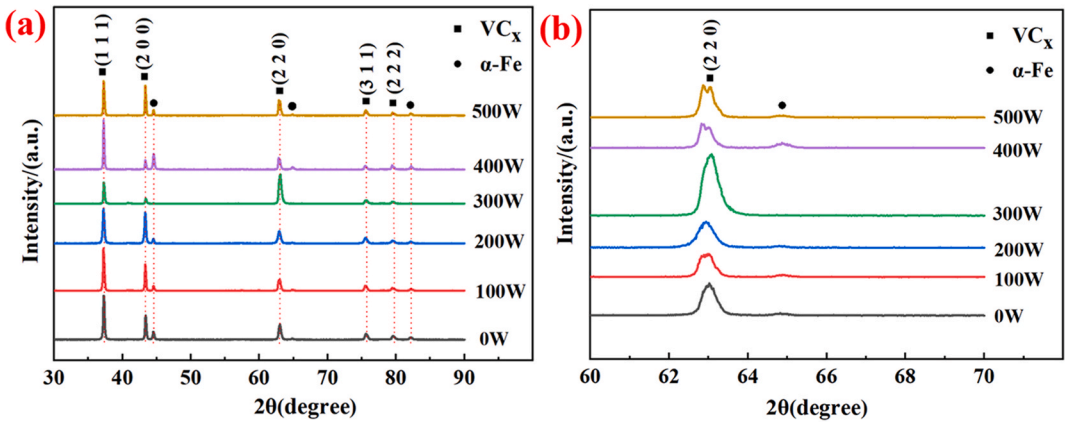

Fig. 7. XRD of vanadizing layers after laser remelting with different powers (a) 30°–90° (b) 60°–70°.

power of 500 W is jagged and the thickness is also the thinnest, which is consistent with the results of metallographic analysis. The main elements of the vanadizing layer obtained by powder embedding vanadizing without laser remelting or after laser remelting are Fe and V, which are the same as those obtained by XRD phase analysis.

Fig. 9 is the cross-section line scan spectrum of vanadizing when the laser remelting power is 300 W. It can be seen that the distribution of elements in the layer and the matrix, and the quantitative comparison of elements can be carried out by the peak intensity of elements. The distribution of elements on this line is different, mainly from the changes of V, Fe and Cr elements, and V elements are mainly concentrated in the layer. Fe element is mainly distributed in the matrix; the Cr element changes obviously at the layer, especially between the interface layer and the matrix, and the content is relatively high. The same reason is that the formation of the vanadizing layer hinders the diffusion of Cr atoms.

3.7. Friction performance analysis of vanadizing layer after different power laser remelting

Fig. 10 (a) is the dynamic friction coefficient of vanadizing samples after different laser power remelting. The Si_3N_4 ceramic ball with a diameter of 6.35 mm was selected as the friction pair. The experimental parameters were as follows: temperature room temperature, time 15 min, rotation radius 3 mm, normal load 10 N, friction speed 0.25 m/s, rotation speed 500 r/min. In the initial stage of friction, the sample will experience a running-in period, at this time, the friction coefficient is relatively low. With the extension of friction time, the friction coefficient increases continuously, and then gradually stabilizes. Because the contact area between the sample and the grinding ball is relatively small in the running-in period, the friction coefficient is relatively low. With the extension of time, the contact area between the sample and the grinding ball gradually increases, and the friction coefficient also increases. When the contact area tends to be stable, the friction coefficient gradually tends to be stable. In the figure, the time from the running-in period to the stable wear stage of the samples with different laser powers is basically the same. Fig. 10 (b) shows the average friction coefficient of the vanadizing samples after different laser power remelting. The average friction coefficient of the samples with laser remelting power of 400 W and 500 W is higher, and the average friction coefficient of the sample with 500 W vanadizing is the highest, which is 0.638. The average friction coefficient of 0 W and 300 W is lower, and the average friction coefficient of the sample with 300 W vanadizing is the lowest, which is 0.356.

3.8. One-stroke scratch experiment

Fig. 11 shows the relationship curve between the acoustic emission signal and the friction force generated by the diamond indenter scratching the surface of the vanadizing layer after laser remelting power of 0 W and 300 W. For the laser remelting power of 0 W vanadizing sample, the friction curve has an inflection point when the loading load is 36.8 N, and the acoustic emission signal curve has an inflection point when the loading load is 15.6 N. For the vanadizing sample with laser remelting power of 300 W, the friction curve has an inflection point when the loading load is 41.59 N, and the acoustic emission signal curve has an inflection point when the loading load is 46.28 N. In the scratch test, because the indenter sliding will squeeze and shear the vanadizing layer, when the compressive stress on the vanadizing layer reaches the critical value, the vanadizing layer will break and peel off. Therefore, the critical pressure can be determined, and the bonding force between the vanadizing layer and the matrix can be obtained, which is the critical load L_c. Y, Xie et al. [25] simulated the formula of critical pressure K and critical load Lc:

$$\sigma_m = \frac{k}{R}\left(\frac{L_c H_f}{H}\right)^{0.5} E_f^{0.3} E^{0.2}$$

k is the coefficient, R is the radius of curvature of the indenter, H_f is the hardness of the layer, E_f is the elastic modulus of the layer, H is the hardness of the matrix, and E is the elastic modulus of the matrix. According to the formula, the critical load L_c of the vanadizing

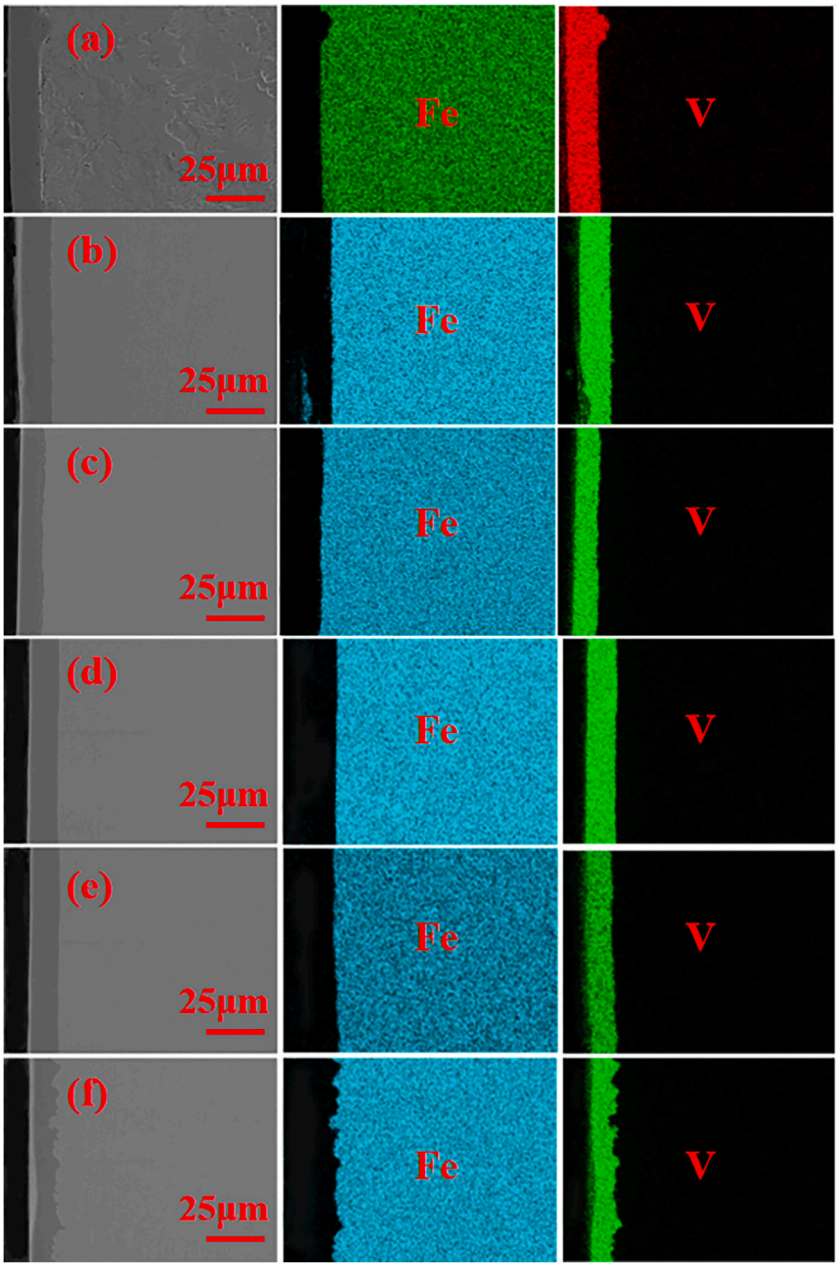

Fig. 8. Scanning electron microscopy and element distribution of vanadizing layer after laser remelting with different powers. (a) 0 W (**b**) 100 W (**c**) 200 W (**d**) 300 W (**e**) 400 W (**f**) 500 W.

sample with laser remelting power of 0 W is 36.8 N. The critical load L_c of the vanadizing sample with laser remelting power of 300 W is 41.59 N.

Fig. 12 (a) and (b) is the single-stroke scratch morphology of vanadizing layers under 0–100 N load scratch. The scratch direction is from bottom to top. When the loading load is close to the maximum value of 100 N, the vanadizing layers with 0 W at both scratch sides and end peel off more compare with that at 300 W. According to Reference [26,27], there is a certain residual compressive stress in the vanadizing layer, which is beneficial to improve to damage resistance. However, when the residual compressive stress exceeds certain strength, the vanadizing layer will be fractured under the action of scratch. The separation of the layer will occur in the edge area of the scratch. The vanadizing layer will peel off at the edge of the scratch. It can be seen from Fig. 12 (b) that the peeling of the vanadizing layer at the edge of the scratch is relatively small, and the bonding ability with the matrix is strong.

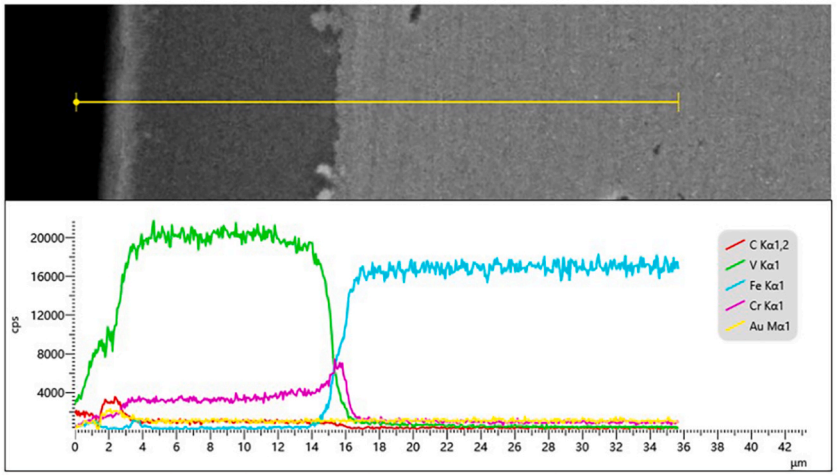

Fig. 9. Vanadizing layer section line scan spectrum (300 W).

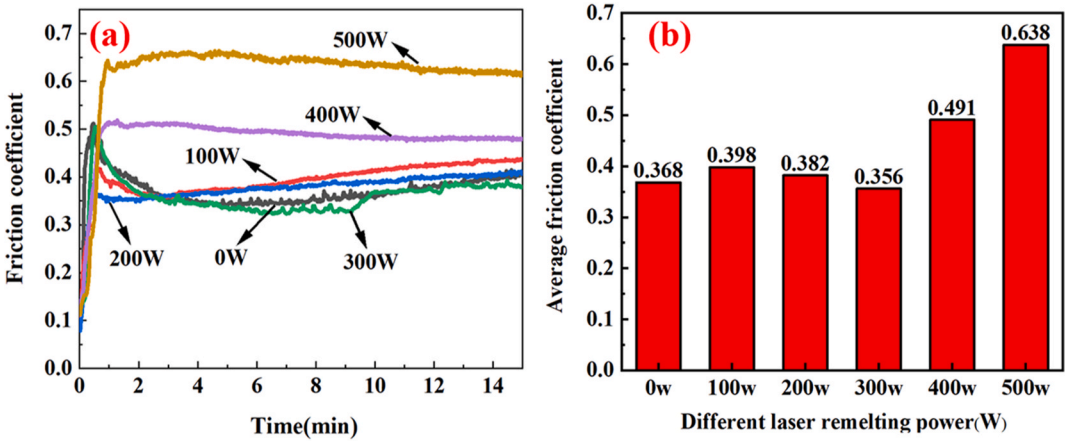

Fig. 10. (a) Dynamic and (b) average friction coefficient of vanadizing layer after laser remelting with different powers.

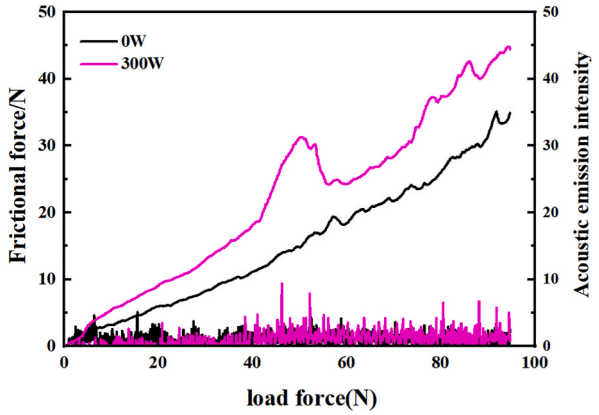

Fig. 11. Scratch acoustic emission signal and friction coefficient curve (a) 0 w, (b) 300 w.

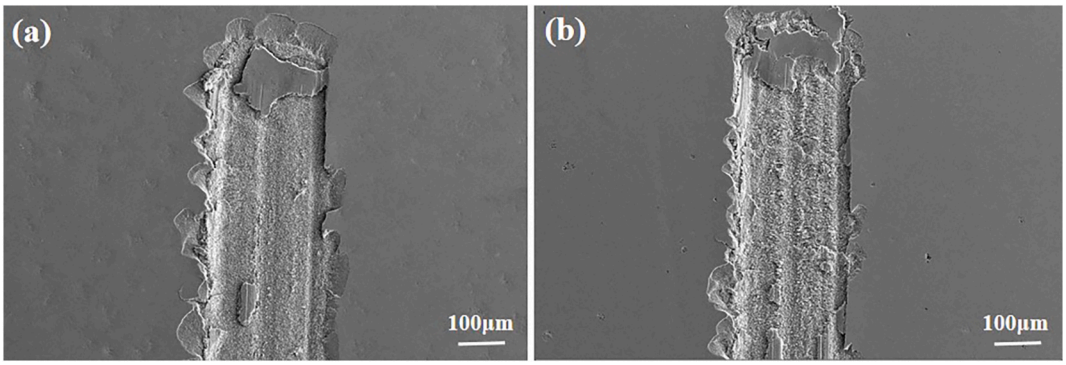

Fig. 12. Morphologies of vanadizing layer after scratch. (a) 0 w, (b) 300 w.

4. Conclusion

1) The remelting zone is obvious when the laser remelting power is 300 W, 400 W and 500 W. When the laser remelting power is 500 W, the microhardness is the highest. Laser remelting does not change the phase composition.
2) The vanadizing layer is mainly composed of VC_x and α-Fe. The thickness of the vanadizing layer decreases first, then increases and then decreases with the increase of laser remelting power. The microhardness of the vanadizing layer increases first and then decreases with the increase of laser remelting power. The average friction coefficient increases first, then decreases and then increases.
3) The laser remelting pre-treatment can change preferred orientation and bonding strength of VC_x layer. When the laser power is 300 W, the laser remelting pretreatment process is the best.

Ethics approval

Not applicable.

Informed consent statement

All the authors have reviewed the manuscript, we agree to publish.

Data availability statement

All data generated or analyzed during this study are included in this article.

CRediT authorship contribution statement

Zhizhong Zeng: Writing – original draft, Validation, Data curation. **Jian Shang:** Resources, Conceptualization. **Dan Lin:** Project administration, Investigation.

Declaration of competing interest

The authors declare that they have no known competing financial interests or personal relationships that could have appeared to influence the work reported in this paper.

Acknowledgements

The authors acknowledge the financial support of the National Natural Science Foundation of China (51405215), Natural Science Foundation of Liao Ning Province (2019-ZD-0703), and Scientific Research Fund of Liaoning Provincial Education Department Grant numbers (2021-LJKZ-0613).

References

[1] Q. Zhao, H. Luo, Z. Pan, X. Wang, H. Cheng, Study on mechanical properties of rare earth elements modified high carbon chromium bearing steel, Mater. Today Commun. 34 (2023) 105329, https://doi.org/10.1016/j.mtcomm.2023.105329.
[2] L. Meng, J. Shang, M. Zhang, A. Xie, Effect of rare earth on microstructure and properties of niobiumizing layer on GCr15 steel for pin shaft, Mater. Res. Express 9 (7) (2022) 076509, https://doi.org/10.1088/2053-1591/ac80a1.

[3] B. Lu, W. Wei, H. Mao, X. Lu, Effect of cold ring rolling on the wear resistance of GCr15 bearing steel after quenching and tempering, Metals 9 (6) (2019) 647, https://doi.org/10.3390/met9060647.
[4] Y. Su, L. Miao, X. Yu, T. Liu, L. Liu, J. Liu, Effect of isothermal quenching on microstructure and hardness of GCr15 steel, J. Mater. Res. Technol. 15 (2021) 2820–2827, https://doi.org/10.1016/j.jmrt.2021.09.096.
[5] L. Wang, P. Qin, Z. Du, Y. Wu, Failure Analysis for Outer Ring Cracking of GCr15 Rolling Bearing, E F A, 2023 107874, https://doi.org/10.1016/j.engfailanal.2023.107874.
[6] Q. Zhao, X. Wang, Z. Pan, W. Ya, H. Cheng, Yi Ma, H. Luo, X. Li, Effects of rare earth elements addition on mechanical properties and corrosion behavior of GCr15 bearing steel under different heat treatment conditions, Corros. Commun. 9 (2023) 65–76, https://doi.org/10.1016/j.corcom.2022.06.004.
[7] S. Li, H. Chen, T. Luo, G. Xiao, M. Yi, Z. Chen, J. Zhang, C. Xu, Tribological properties of laser surface texturing modified GCr15 steel under graphene/5CB lubrication, J. Mater. Res. Technol. 18 (2022) 3598–3611, https://doi.org/10.1016/j.jmrt.2022.04.030.
[8] R.K. Sinha, Y. Nagpal, R. Sharma, N. Kumar, Investigation on corrosion characteristics of SS316L by thermal spray coating technique using Ni-80Cr alloy, J. Phys. Chem. Solid. 2178 (1) (2022) 12–32, https://doi.org/10.1088/1742-6596/2178/1/012032.
[9] F. Frank, M. Tkadletz, C. Czettl, N. Schalk, Microstructure and mechanical properties of zrn, zrcn and zrc coatings grown by chemical vapor deposition, Coatings 11 (5) (2021) 491, https://doi.org/10.3390/coatings11050491.
[10] Z. Joska, Z. Pokorný, J. Kadlec, Z. Studený, E. Svoboda, Hardness of nitrided layers treated by plasma nitriding, Acta Polytech. CTU Proc. 27 (2020) 53–56, https://doi.org/10.14311/APP.2020.27.0053.
[11] Q. Wang, Y. Tang, R. Pei, Y. Xi, S. Wan, A study on preparation and corrosion behavior of nano rare earth oxide-modified chromized coatings, Mater. Corros. 71 (2) (2020) 249–257, https://doi.org/10.1002/maco.201911017.
[12] Y. Yang, J. Li, F. Yao, X. Li, Effect of laser remelting on the organization and properties of WC/Ni-based coatings generated in situ by laser cladding, J. Manuf. Process. 102 (2023) 501–512, https://doi.org/10.1016/j.jmapro.2023.07.075.
[13] N. Zhao, R. Shan, L. Wang, et al., Bonding properties and corrosion resistance of TaC-Fe enhanced layer on GCr15 surface prepared by in-situ hot pressing[J], J. Alloys Compd. 940 (2023) 168489, https://doi.org/10.1016/j.jallcom.2022.168489.
[14] J. Chen, Z. Li, Y. Chu, J. Chen, X. Shen, Microstructure distribution and grain coarsening model of GCr15 steel in the laser surface treatment, Metals Mater. Int. Met. Mater. Int. 28 (10) (2022) 2318–2329, https://doi.org/10.1007/s12540-021-01148-7.
[15] T. Dong, P. Lu, Q. Ma, G. Li, Q. Liu, B. Fu, J. li, Effect of laser remelting on high-temperature oxidation resistance of AlCoCrFeNi high-entropy alloy coating, Surf. Cat. Tech. 466 (2023) 129608, https://doi.org/10.1016/j.surfcoat.2023.129608.
[16] J. Shang, M. Zhang, S. Tan, A. Xie, L. Meng, Y. Zhang, Improved wear and hot melting loss resistance of a vanadizing carbide layer prepared on H13 steel, Mater. Lett. 337 (2023) 133967, https://doi.org/10.1016/j.matlet.2023.133967.
[17] L. Meng, J. Shang, M. Zhang, A. Xie, Growth kinetics and mechanical properties of rare-earth vanadizingizing layer on GCr15 steel, Surf. Coat. 12 (7) (2022) 1018, https://doi.org/10.3390/coatings12071018.
[18] C.T. Kwok, F.T. Cheng, H.C. Man, Microstructure and corrosion behavior of laser surface-melted high-speed steels, Surf. Coating. Technol. 202 (2) (2007) 336–348, https://doi.org/10.1016/j.surfcoat.2007.05.085.
[19] A. Moradiani, Z.M. Beiranvand, R.C. Ratnayake, A. Aliabadi, M. Rasoulinia, The effect of laser surface melting on the retained austenite and wear properties of AISI D2 tool steel, Optik 252 (2022) 168469, https://doi.org/10.1016/j.ijleo.2021.168469.
[20] D.P. Karmakar, M. Gopinath, A.K. Nath, Effect of tempering on laser remelted AISI H13 tool steel, Surf. Coating. Technol. 361 (2019) 136–149, https://doi.org/10.1016/j.surfcoat.2019.01.022.
[21] P. Yu, H. Yuan, F. Ge, T. Peng, Q. Gao, S. Guo, S. Guan, H. Liu, J. Guan, X. Liu, Microstructure and properties of $AlCoCrFeNiNb_x$ (x= 0, 0.1 and 0.5) high-entropy alloys enhanced by laser remelting, Mater. Char. 199 (2023) 112784, https://doi.org/10.1016/j.matchar.2023.112784.
[22] Z. Chong, Y. Sun, J. Wang, W. Cheng, L. Huang, C. Han, X. Ma, Laser remelting induces grain refinement and properties enhancement in high-speed laser cladding AlCoCrFeNi high-entropy alloy coatings, Intermetallics 150 (2022) 107686, https://doi.org/10.1016/j.intermet.2022.107686.
[23] X. Fan, Z. Yang, C. Zhang, Y. Zhang, H. Che, Evaluation of vanadizing carbide coatings on AISI H13 obtained by thermo-reactive deposition/diffusion technique, Surf. Cat. Tech. 205 (2) (2010) 641–646, https://doi.org/10.1016/j.surfcoat.2010.07.065.
[24] C.K.N. Oliveira, C.L. Benassi , L, C. Casteletti, Evaluation of hard coatings obtained on AISI D2 steel by thermo-reactive deposition treatment, Surf. Cat. Tech. 201 (3) (2006) 1880–1885, https://doi.org/10.1016/j.surfcoat.2006.03.036.
[25] Y. Xie, H.M. Hawthorne, A model for compressive coating stresses in the scratch adhesion test, Surf. Cat. Tech. 141 (1) (2001) 15–25, https://doi.org/10.1016/S0257-8972(01)01130-6.
[26] S.J. Bull, E.G. Berasetegui, An overview of the potential of quantitative coating adhesion measurement by scratch testing, Tribol. Int. 39 (2) (2006) 99–114, https://doi.org/10.1016/j.triboint.2005.04.013.
[27] I. Campos-Silva, M.N. Granados-Vázquez, A.D. Contla-Pacheco, G. Luis-Pantoja, L.E. Castillo-Vela, A. Contreras-Hernández, A. Meneses-Amador, Improving boride layer adhesion to AISI D2 steel by post-heat treatments, T. Indian I. Metals (2023) 1–10, https://doi.org/10.1007/s12666-023-03006-z.